Journal of Biomolecular NMR, 6 (1995) 347–360
ESCOM

J-Bio NMR 315

Internal mobility of cyclic RGD hexapeptides studied by ^{13}C NMR relaxation and the model-free approach

Jacques Briand* and Kenneth D. Kopple

Department of Physical and Structural Chemistry, UW-2940, SmithKline Beecham Pharmaceuticals, 709 Swedeland Road, King of Prussia, PA 19406-0939, U.S.A.

Received 21 June 1995
Accepted 1 September 1995

Keywords: ^{13}C NMR relaxation; Arg-Gly-Asp (RGD) peptide; Internal motion; Model-free formalism

Summary

The internal mobility of three isomeric cyclic RGD hexapeptides designed to contain two β-turns in defined positions, cyclo(Arg-Gly-Asp-Gly-D-Pro-Pro) (**I**), cyclo(Arg-Gly-Asp-D-Pro-Gly-Pro) (**II**) and cyclo(Arg-Gly-Asp-D-Pro-Pro-Gly) (**III**), have been studied by ^{13}C NMR longitudinal and transverse relaxation experiments and measurements of steady-state heteronuclear $\{^1H\}$-^{13}C NOE enhancement with ^{13}C at natural abundance. The data were interpreted according to the model-free formalism of Lipari and Szabo, which is usually applied to data from macromolecules or larger sized peptides with overall rotational correlation times exceeding 1 ns, to yield information about internal motions on the 10–100 ps time scale. The applicability of the model-free analysis with acceptable uncertainties to these small peptides, with overall rotational correlation times slightly below 0.3 ns, was demonstrated for this specific instance. Chemical exchange contributions to T_2 from slower motions were also identified in the process. According to the order parameters obtained for its backbone α-carbon atoms, **II** has the most rigid backbone conformation on the 10–100 ps time scale, and **I** the most flexible. This result coincides with the results of earlier NMR-constrained conformational searches, which indicated greatest uncertainty in the structure of **I** and least in **II**.

Introduction

The study of conformational flexibility in biomolecules has in recent years been the subject of considerable interest. Much of the impetus to characterize these motional phenomena has been motivated by the important role they are believed to play in the biochemical function of biomolecules (Williams, 1989). Another incentive is the need to estimate the level of misinterpretation or inconsistencies in static structure calculations based upon the use of distance geometry and molecular dynamics methods, in conjunction with internuclear distance and backbone dihedral angle constraints derived from NMR measurements (Bonvin et al., 1993).

The structural ambiguity brought about by the wide range of likely conformations sometimes observed for parts of biomolecules may or may not be a matter of internal flexibility. For instance, experimental constraints that can be shown to result from a mixed population of conformers interconverting on a fast NMR time scale may rightly be associated to intrinsic internal mobility (Blackledge et al., 1993). On the other hand, a lack of experimental constraints unrelated to intrinsic flexibility may give the appearance of internal motions. The first case is particularly relevant for small- and mid-sized peptides.

We encountered such a structural ambiguity with the first of three isomeric cyclic RGD hexapeptides, cyclo(Arg-Gly-Asp-Gly-D-Pro-Pro) (**I**), cyclo(Arg-Gly-Asp-D-Pro-Gly-Pro) (**II**) and cyclo(Arg-Gly-Asp-D-Pro-Pro-Gly) (**III**), which differ only in the position of the second glycine residue. These three synthetic cyclic peptides of limited conformational mobility were part of an investigation for probing the biologically active conformations of Arg-

*To whom correspondence should be addressed.

Gly-Asp-containing peptides used as inhibitors of platelet aggregation (Ali and Samanen, 1992; Peishoff et al., 1992).

It was anticipated and confirmed experimentally by a NOE-constrained search that **I** and **III** would adopt a two-β-turn cyclic hexapeptide backbone conformation containing a D-Pro-L-Pro type II' β-turn (Bean et al., 1992) on one side of the hexapeptide ring, and a Gly-Asp β-turn for **I**, or Gly-Arg β-turn for **III**, across the ring. For **II** it was anticipated, and also confirmed experimentally, that the backbone would adopt a turn-extended-turn RGD conformation containing Pro-Arg and Asp-D-Pro β-turns (Peishoff et al., 1992). However, as shown in Fig. 1, the constrained search yielded a narrower range of likely conformations for **II** and **III** than for **I**, despite the fact that all three peptides yielded experimentally a similar number of NOE distance constraints. The observed structural ambiguity observed for **I** reflects the fact that the constrained search could not indicate, for the Gly-Asp sequence, a preference among the structures with type I, II, II' and III β-turns.

All three peptides were observed to give spectra with narrow line widths down to 213 K; for all three of them, line broadening began to occur at lower temperatures. The similarity in this regard suggests that the apparent difference in flexibility implied by the constrained search was not paralleled by differences in activation energy barriers to backbone conformation exchange in the 10 kcal/mol region, i.e., the millisecond time scale at 200 K. Furthermore, for **I** no differences were observed for spin-lock decays of ^{13}C transverse magnetization of backbone aliphatic ^{13}C nuclei using different rf field strengths. However, these results are not conclusive, because by such experiments one cannot exclude the presence of motional processes on the microsecond time scale with sufficiently small chemical shift differences between conformers.

An approach that has proved very useful for characterizing the internal dynamics of proteins (Kay et al., 1989; Clore et al., 1990a; Barbato et al., 1992; Schneider et al., 1992; Stone et al., 1992) and mid-sized peptides (Dellwo and Wand, 1989; Palmer et al., 1991; Zieger and Sterk, 1992; Jarvis and Craik, 1995) with rate constants comparable to the Larmor frequency has been to measure laboratory frame ^{15}N or ^{13}C longitudinal and transverse relaxation times, combined with heteronuclear NOE enhancements, and to interpret them in the context of the 'model-free' formalism (Lipari and Szabo, 1982). In this approach, the heteronuclear relaxation rates are assumed to depend, via dipolar relaxation, on the dynamics of the heteronucleus–proton vectors with respect to the external magnetic field. The internal motion is described in terms of an effective correlation time and a generalized order parameter characterizing the amplitude of that local motion. Although slow motional processes can also lead to measurable effects on the transverse T_2 relaxation time,

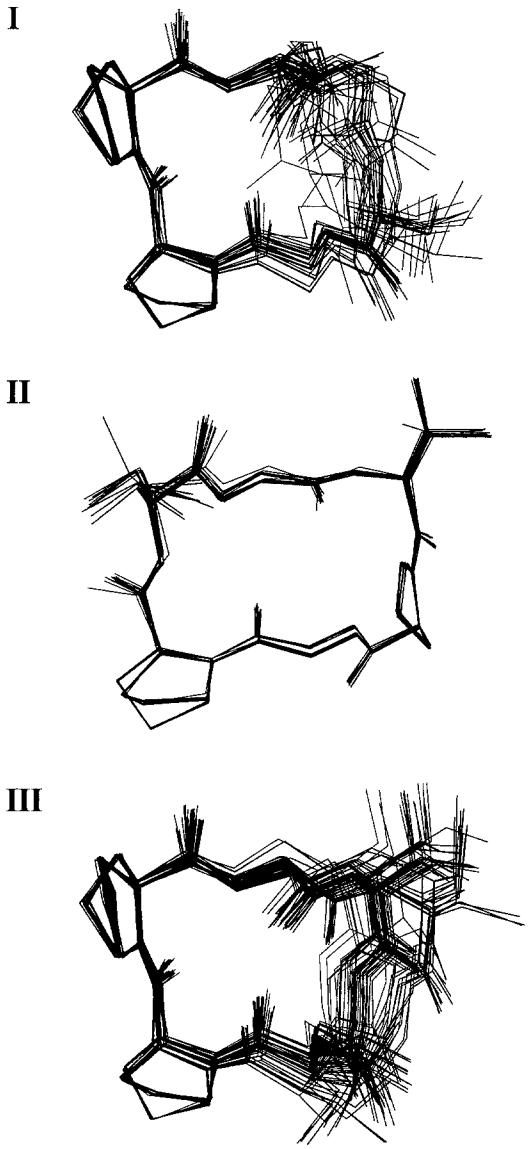

Fig. 1. Structures for three isomeric cyclic hexapeptides, obtained by a NOE-constrained distance geometry search and energy minimization (Bean et al., 1992; Peishoff et al., 1992). Only structures within 4 kcal/mol of the lowest energy structure returned by the search are depicted. For **I**, the NOE constraints were compatible with type I, II, II' and III β-turns at the Gly-Asp sequence; 22 structures are displayed. For **II**, only type I turns at L-Pro-Arg and I' turns at Asp-D-Pro were found; 31 structures are displayed. For **III**, the Arg-Gly sequence is best described by type II and III' β-turns; 59 structures are displayed, among which 45 structures are described by the former turn and 14 structures by the latter turn. Compound **II** has the narrowest range of likely conformations, followed by compound **III**, which appears to have two classes of likely conformations; finally, compound **I** seems to exhibit a 'continuum' of likely conformations at the Gly-Asp sequence.

the relaxation data can still be interpreted by introducing an exchange term R_{ex}, which is a loose term containing all the contributions from motional processes that are slow compared to the Larmor frequency time scale. To gain more insight, the generalized order parameter can then be interpreted in the context of a particular motional model

such as the 'wobbling-in-a-cone' model (Lipari and Szabo, 1980; Richarz et al., 1980). Typically, the effective correlation times for these fast motions observed with the model-free approach are of the order of 10–100 ps.

A modified version of the model-free approach (Clore et al., 1990b) adds two additional degrees of freedom in the form of a second effective correlation time, slow compared to the first one and typically in the same range as the overall correlation time, and its corresponding generalized order parameter, which is a measure of its contribution. Although it was shown to be useful, this modified version has to be used with care to avoid overinterpretation of the relaxation data, since the number of independent measurements is smaller compared to the number of dynamical parameters required.

These approaches make the assumption that the spectral density function of the heteronucleus–proton bond motion can be described by a sum of Lorentzian functions, the amplitudes and time constants of which are adjusted to best fit the observed relaxation data. This assumption is perfectly justifiable and reasonable if the motion is Markovian (King and Jardetzky, 1978). A recently introduced, more direct approach (Peng and Wagner, 1992a,b) evaluates from a set of relaxation data the spectral density functions sampled at five different frequencies without any a priori assumption on the functional form of the spectral density function. This approach may be considered as being more rigorous, since it does not necessitate any model assumption on the spectral density functions. However, it requires the measurement of six different kinds of relaxation rates and, in the end, it still remains desirable to interpret these extracted spectral density values in the context of a specific motional model.

The current work describes a ^{13}C NMR relaxation study performed on our three synthetic cyclic hexapeptides, which have been analyzed in terms of the model-free approach. Our aim is to investigate the internal dynamics on a time scale observable with the model-free approach and to verify whether observed differences in the internal dynamics are consistent with the conclusions from the conformational search.

Theory

Dipolar relaxation

The relaxation of aliphatic ^{13}C nuclei at natural abundance is mediated predominantly by dipolar interactions with directly bound protons. Chemical shift anisotropy, which is typically in the 20–25 ppm range for aliphatic ^{13}C nuclei (Bremi et al., 1994), will be assumed below to be a negligible relaxation mechanism. The T_1 and T_2 relaxation times for dipolar relaxation when n protons are attached to the ^{13}C nucleus with identical bond lengths r_{CH} are given by (Abragam, 1961):

$$\frac{1}{T_1} = R_1 = nq_{CH}[J(\omega_H - \omega_C) + 3J(\omega_C) + 6J(\omega_H + \omega_C)] \quad (1)$$

$$\frac{1}{T_2} = R_2 = n\frac{q_{CH}}{2}[4J(0) + J(\omega_H - \omega_C) + 3J(\omega_C) + 6J(\omega_H) + 6J(\omega_H + \omega_C)] \quad (2)$$

with $q_{CH} = (\mu_0/4\pi)^2(\gamma_H\gamma_C h/2\pi)^2/(20r_{CH}^6)$. The expression for T_1 corresponds to our experimental conditions, where ^{13}C relaxation takes place in the presence of broadband ^1H decoupling. Cross-relaxation effects (Neuhaus and Williamson, 1989) can thus be ignored and T_1 relaxation will be monoexponential. The steady-state heteronuclear $\{^1H\}$-^{13}C NOE enhancement is given by:

$$NOE = \left(\frac{\gamma_H}{\gamma_C}\right)\frac{6J(\omega_H + \omega_C) - J(\omega_H - \omega_C)}{J(\omega_H - \omega_C) + 3J(\omega_C) + 6J(\omega_H + \omega_C)} \quad (3)$$

The spectral density function, $J(\omega)$, is the Fourier transform of the reorientational autocorrelation function of the C-H internuclear vector and embodies the molecular motion dynamics sampled at various frequencies. The values of the constants used in Eqs. 1–3 are: $\mu_0 = 4\pi \times 10^{-7}$ T m A^{-1}, $h = 6.62618 \times 10^{-34}$ J s, $\gamma_H = 2.675062 \times 10^8$ T s^{-1}, $\gamma_C = 6.726229 \times 10^7$ T s^{-1} and $r_{CH} = 1.1 \times 10^{-10}$ m. The two B_0 field strengths used for computing ω_H and ω_C at different field strengths are 11.744 T and 9.395 T.

Chemical exchange contribution to T_2

The expression for T_2 ignores chemical or conformational exchange contributions that may decrease its apparent value and lead to inconsistencies in its interpretation. A more accurate description of T_2 includes the dipolar contribution term T_{2D}, expressed by Eq. 2, and an exchange term R_{ex}:

$$\frac{1}{T_2} = \frac{1}{T_{2D}} + R_{ex} \quad (4)$$

For chemical exchange between two equally populated sites, the R_{ex} contribution to the T_2 decay of the spin-echo amplitudes in the context of a CPMG experiment (Carr and Purcell, 1954; Meiboom and Gill, 1958) is given by (Bloom et al., 1965):

$$R_{ex} = k_{ex} - \frac{1}{2\tau}\sinh^{-1}\left\{\frac{k_{ex}}{(k_{ex}^2 - \omega_{ex}^2)^{1/2}}\sinh\left[2(k_{ex}^2 - \omega_{ex}^2)^{1/2}\tau\right]\right\} \quad (5)$$

if $k_{ex} > \omega_{ex}$, where k_{ex} is the exchange rate constant, ω_{ex} is the chemical shift difference between the two exchanging sites, and 2τ is the pulse spacing between two consecutive 180° pulses in the CPMG sequence. For the long τ limit,

$\sinh[2(k_{ex}^2 - \omega_{ex}^2)^{1/2}\tau] \gg 1$, and very fast exchange, $k_{ex} \gg \omega_{ex}$, R_{ex} reduces to:

$$R_{ex} \approx \frac{\omega_{ex}^2}{2k_{ex}} \quad (6)$$

For the short τ limit, $k_{ex}\tau \ll 1$ and $\omega_{ex}\tau \ll 1$, the exchange contribution to T_2 becomes negligible and is approximately $R_{ex} \approx 2/3 k_{ex} \omega_{ex}^2 \tau^2$.

Model-free formalism

In the model-free formalism of Lipari and Szabo, the autocorrelation function, C(t), is based on a simple form and is defined as the product of two independent correlation functions, $C(t) = C_0(t)\,C_i(t)$, where $C_0(t) = e^{-t/\tau_m}$ represents the overall reorientational molecular tumbling with a correlation time, τ_m, for an isotropically tumbling molecule, and $C_i(t) = S^2 + (1 - S^2)e^{-t/\tau_e}$ represents the internal dynamics. The form of $C_i(t)$ has been defined in a model-independent way by a single exponential approximation with the asymptotic boundary $C_i(t \to \infty) = S^2$. S^2 is the so-called 'generalized order parameter' reflecting the degree of spatial restriction of the internal motion, and τ_e is an effective correlation time which is a measure of the rate of the internal motion. $C_0(t)$ pertains to all one-bond C-H internuclear vectors, whereas $C_i(t)$ is specific to a particular one-bond C-H internuclear vector within the molecule. The corresponding spectral density function is given by:

$$J(\omega) = S^2 \frac{2\tau_m}{1 + \omega^2\tau_m^2} + (1 - S^2)\frac{2\tau}{1 + \omega^2\tau^2} \quad (7)$$

with $1/\tau = 1/\tau_m + 1/\tau_e$. It should be noted from Eq. 7 that, depending upon the ratio between τ_e and τ_m, one may not be able to accurately measure or even time resolve τ_e by relaxation experiments based on coupling to the overall tumbling. The observability condition is approximately (Bremi et al., 1994) $0.1\tau_m < \tau_e < 10\,\tau_m$. Although S^2 can more easily be interpreted in a model-independent way than τ_e, i.e., $S^2 = 1$ in the absence of internal motion, and $S^2 \ll 1$ for weakly restricted internal motion, both parameters can be physically interpreted within the framework of various motional models.

Experimental Methods

Synthesis and sample preparation

Synthetic details and characterization of the peptides have been reported elsewhere (Ali and Samanen, 1992). Sample solutions of about 30, 35 and 25 mM for **I**, **II** and **III**, respectively, in methyl-d_3 alcohol with ^{13}C at natural abundance (MSD Isotopes, Montreal) were used. The chemical shift position of the OH proton of the solvent, as determined from the rf carrier position for solvent presaturation, was identical for all three samples to within 0.1 Hz.

NMR measurements

All experiments were performed on Bruker AMX consoles with a sample temperature of 293 K. The steady-state heteronuclear $\{^1H\}$-^{13}C NOE enhancement and ^{13}C T_2 relaxation experiments were carried out at 500 MHz proton resonance frequency. T_1 relaxation measurements were carried out at both 400 and 500 MHz proton resonance frequency. The sample concentrations and the spectral resolution were sufficient to collect all the spectra by direct observation of ^{13}C using one-dimensional techniques. Only a few aliphatic ^{13}C resonances were obscured by the residual septuplet resonance of methyl-d_3 alcohol; these included the C^δ of the proline and D-proline residues, and the aspartate C^α of **III**. For the latter, which was of significant interest (see later), attempts by indirect detection techniques were made, but the aspartate H^α also overlapped with the residual proton signal of the solvent.

The spin–lattice relaxation times, T_1, were measured by the standard inversion–recovery method (Vold et al., 1968) with broadband ^1H decoupling during the whole experiment. Twelve T_1 relaxation delays of 0.1, 100, 300, 500, 750, 1000, 1250, 1500, 2000, 3000, 4000 and 5000 ms were used. A recovery delay (including data acquisition) between experiments of at least $5T_1$ of the longest measured T_1 was used.

The spin–spin relaxation times, T_2, were measured using a Carr–Purcell–Meiboom–Gill (CPMG) pulse train of ^{13}C 180° refocusing pulses during the relaxation delay. Since the chemical shift anisotropy was sufficiently small (Palmer et al., 1991) for the aliphatic ^{13}C nuclei considered in this study, no ^1H 180° refocusing pulses during the relaxation delay were applied (Kay et al., 1992; Palmer et al., 1992) for suppressing cross-correlation between ^1H-^{13}C dipolar and ^{13}C chemical shift anisotropy interactions. Furthermore, a pulse spacing 2τ of 1 ms between two consecutive ^{13}C 180° pulses in the CPMG sequence was judged adequate (Palmer et al., 1993) to minimize the effects of antiphase coherence evolution (Peng et al., 1991; Kay et al., 1992; Palmer et al., 1992). Twelve spectra were acquired, using relaxation delays of 12, 36, 72, 120, 180, 240, 300, 360, 420, 480, 540 and 600 ms. Broadband ^1H decoupling was used during data acquisition and the recovery delay. The length of the latter was similar to the one used during the T_1 experiments.

For the steady-state heteronuclear $\{^1H\}$-^{13}C NOE measurements, three separate pairs of spectra were acquired with and without ^1H saturation during the recovery delay. A recovery delay similar to that used in the T_1 experiments was employed. The WALTZ-16 pulse sequence (Shaka et al., 1983) was used for decoupling during data acquisition for all relaxation and NOE experiments and for proton saturation during the recovery delay.

TABLE 1
^{13}C CHEMICAL SHIFTS, RELAXATION TIMES AND $\{^1H\}$-^{13}C NOE ENHANCEMENTS FOR cyclo(Arg-Gly-Asp-Gly-D-Pro-Pro) (I)

Residue	^{13}C assignment (ppm)	nT_1 (s)		nT_2 (s)	NOE	T_1/T_2
		^1H 400 MHz	^1H 500 MHz	^1H 500 MHz	^1H 500 MHz	^1H 500 MHz
Backbone						
Arg[1] α	53.4	0.387±0.027	0.398±0.011	0.325±0.038	1.411±0.028	1.225±0.147
Gly[2] α	45.1	0.449±0.037	0.506±0.018	0.384±0.032	1.488±0.031	1.318±0.119
Asp[3] α	50.7	0.371±0.029	0.423±0.014	0.173±0.014	1.413±0.030	2.445±0.214
Gly[4] α	42.7	0.486±0.041	0.539±0.018	0.446±0.038	1.496±0.031	1.209±0.111
D-Pro[5] α	62.0	0.369±0.025	0.455±0.012	0.364±0.049	1.461±0.027	1.250±0.171
Pro[6] α	60.0	0.413±0.027	0.496±0.012	0.369±0.045	1.498±0.026	1.344±0.167
Side chains						
Arg[1] β	31.7	0.429±0.041	0.515±0.017	0.354±0.028	1.569±0.032	1.455±0.125
Asp[3] β	35.7	0.478±0.104	0.615±0.080	0.043±0.015	1.249±0.097	14.302±5.325
D-Pro[5] β	30.4	0.549±0.041	0.639±0.019	0.524±0.049	1.527±0.029	1.219±0.120
Pro[6] β	29.0	0.688±0.044	0.786±0.020	0.611±0.059	1.504±0.026	1.286±0.128
Arg[1] γ	26.3	0.600±0.045	0.630±0.017	0.526±0.043	1.597±0.027	1.198±0.103
D-Pro[5] γ	24.9	0.571±0.044	0.743±0.024	0.572±0.059	1.478±0.028	1.299±0.140
Pro[6] γ	26.4	0.752±0.047	0.901±0.021	0.787±0.104	1.430±0.024	1.145±0.154
Arg[1] δ	41.9	0.555±0.039	0.660±0.018	0.557±0.050	1.601±0.028	1.185±0.111

NMR data processing

All the NMR spectra were processed with the FELIX software package, v. 2.05 (Biosym Technologies, Inc., San Diego, CA). An exponential apodization with a line broadening of 3 Hz for **I** and **II** and 2 Hz for **III** was used, and all spectra were Fourier transformed with a digital resolution of about 0.2 Hz. The use of a slightly smaller line-broadening apodization for **III** was necessary for resolving some very close ^{13}C resonances. The relaxation times and NOE enhancements were calculated by extracting peak heights from carefully baseline-corrected ^{13}C spectra. The longitudinal relaxation times were calculated from an inversion-recovery curve, least-squares fitted to a three-parameter monoexponential function. Transverse relaxation times were calculated from a decay curve, least-squares fitted to a two-parameter monoexponential function. The parameters were optimized by using a downhill simplex function minimizer (Press et al., 1986). The experimental error in every measured peak height was estimated by evaluating the root-mean-square baseline noise of the spectrum from which it was extracted. The covariance matrix of the fitted parameters, assuming uncorrelated measurement errors of equal variance, was used for estimating the experimental error in the relaxation times.

The experimental error in the NOE enhancement was calculated by standard propagation error techniques (Bevington, 1969):

$$\sigma_{NOE} = \frac{1}{\sqrt{N}} \sqrt{\sum_{i=1}^{N} \frac{A_i^2}{B_i^2} \left(\frac{\sigma_{A_i}^2}{A_i^2} + \frac{\sigma_{B_i}^2}{B_i^2} \right)} \qquad (8)$$

where N refers to the number of independent pairs of experiments and A and B are the resonance peak heights with and without ^1H saturation, respectively, during the recovery delay. Three such pairs of experiments were acquired and the NOE enhancements were calculated from the average NOE (NOE = (A/B) − 1) values. The resulting NOE enhancements and relaxation times, together with their estimated experimental errors, are given in Tables 1, 2 and 3 for compounds **I**, **II** and **III**, respectively.

Evaluation of the dynamical parameters

The model-free parameters were evaluated from the relaxation times and NOE enhancements by minimization of the following error function:

$$\begin{aligned} E^2 = \sum_{i=1}^{N} E_i^2 = \sum_{i=1}^{N} & \left(\frac{T_1^{calc}(\omega_{0,2},i) - T_1^{exp}(\omega_{0,2},i)}{\sigma_1(\omega_{0,2},i)} \right)^2 \\ & + \left(\frac{T_1^{calc}(\omega_{0,1},i) - T_1^{exp}(\omega_{0,1},i)}{\sigma_1(\omega_{0,1},i)} \right)^2 \\ & + \left(\frac{NOE^{calc}(\omega_{0,1},i) - NOE^{exp}(\omega_{0,1},i)}{\sigma_{NOE}(\omega_{0,1},i)} \right)^2 \\ & + \left\{ \left(\frac{T_2^{calc}(\omega_{0,1},i) - T_2^{exp}(\omega_{0,1},i)}{\sigma_2(\omega_{0,1},i)} \right)^2 \right\}_{optional} \end{aligned} \qquad (9)$$

where the sum runs over all the considered ^{13}C nuclei, including both the backbone and the side-chain nuclei. The $\sigma_1(\omega_{0,2},i)$, $\sigma_1(\omega_{0,1},i)$, $\sigma_2(\omega_{0,1},i)$ and $\sigma_{NOE}(\omega_{0,1},i)$ are, respectively, the experimental errors in T_1 at 400 MHz proton resonance frequency and T_1, T_2 and NOE at 500 MHz proton resonance frequency for the *i*th nucleus. However, the inclusion of T_2 in the minimization of E^2

TABLE 2
^{13}C CHEMICAL SHIFTS, RELAXATION TIMES AND $\{^1H\}$-^{13}C NOE ENHANCEMENTS FOR cyclo(Arg-Gly-Asp-D-Pro-Gly-Pro) (**II**)

Residue	^{13}C assignment (ppm)	nT_1 (s)		nT_2 (s)	NOE	T_1/T_2
		^1H 400 MHz	^1H 500 MHz	^1H 500 MHz	^1H 500 MHz	^1H 500 MHz
Backbone						
Arg[1] α	53.1	0.332 ± 0.012	0.377 ± 0.006	0.345 ± 0.022	1.537 ± 0.023	1.093 ± 0.072
Gly[2] α	42.1	0.422 ± 0.021	0.472 ± 0.009	0.424 ± 0.020	1.462 ± 0.027	1.113 ± 0.057
Asp[3] α	51.6	0.345 ± 0.014	0.363 ± 0.006	0.309 ± 0.018	1.427 ± 0.023	1.175 ± 0.071
D-Pro[4] α	62.3	0.375 ± 0.013	0.407 ± 0.006	0.387 ± 0.027	1.433 ± 0.021	1.052 ± 0.075
Gly[5] α	42.8	0.358 ± 0.019	0.436 ± 0.009	0.406 ± 0.020	1.522 ± 0.028	1.074 ± 0.057
Pro[6] α	63.4	0.364 ± 0.013	0.407 ± 0.006	0.383 ± 0.028	1.429 ± 0.022	1.063 ± 0.079
Side chains						
Arg[1] β	28.6	0.452 ± 0.022	0.501 ± 0.009	0.456 ± 0.022	1.584 ± 0.026	1.099 ± 0.057
Asp[3] β	36.0	0.560 ± 0.027	0.575 ± 0.010	0.423 ± 0.019	1.672 ± 0.027	1.359 ± 0.065
D-Pro[4] β	30.1	0.649 ± 0.026	0.721 ± 0.012	0.664 ± 0.044	1.438 ± 0.023	1.086 ± 0.074
Pro[6] β	30.9	0.665 ± 0.025	0.733 ± 0.011	0.691 ± 0.043	1.493 ± 0.022	1.061 ± 0.068
Arg[1] γ	26.6	0.603 ± 0.025	0.652 ± 0.010	0.621 ± 0.034	1.568 ± 0.022	1.050 ± 0.060
D-Pro[4] γ	25.5	0.771 ± 0.031	0.854 ± 0.013	0.805 ± 0.064	1.556 ± 0.023	1.061 ± 0.086
Pro[6] γ	25.8	0.860 ± 0.030	0.929 ± 0.013	0.906 ± 0.078	1.591 ± 0.021	1.025 ± 0.089
Arg[1] δ	41.8	0.613 ± 0.022	0.708 ± 0.010	0.658 ± 0.035	1.687 ± 0.022	1.076 ± 0.059

may yield unreliable results because, as noted earlier, the observed T_2 relaxation times may be subject to additional shortening due to processes of conformational or chemical exchange on time scales much longer than the sensitive range of the model-free approach. Two schemes were used to circumvent this problem. The first one is to exclude T_2 from the minimization procedure and then compare the T_2 values predicted by the model-free parameters with those obtained experimentally. The alternative is to estimate which T_2 values may be subject to line broadening and exclude them from the minimization. We have compared the results of the two procedures for self-consistency.

The minimization of E^2 was based on a grid search in which τ_m (Eq. 7) was varied stepwise but held constant, while for each nucleus a two-dimensional grid search of the internal model-free parameters $\{S^2, \tau_e\}$ was performed. E^2 was thus calculated for each τ_m with its respective set of N optimized pairs of model-free parameters $\{S^2, \tau_e\}$. The optimized τ_m corresponded to the smallest value of E^2. The grid search was performed over the ranges $0 \le S^2 \le 1$, $-11 \le \log(\tau_e) \le -9$ and $-10 \le \log(\tau_m) \le -9$, in steps of 0.01, yielding a total of $101 \times 201 \times 101$ combinations for each nucleus. For τ_m and τ_e, a grid step of 0.01 on a logarithmic scale yields a ratio of 1.023 between two consecutive correlation time values.

TABLE 3
^{13}C CHEMICAL SHIFTS, RELAXATION TIMES AND $\{^1H\}$-^{13}C NOE ENHANCEMENTS FOR cyclo(Arg-Gly-Asp-D-Pro-Pro-Gly) (**III**)

Residue	^{13}C assignment (ppm)	nT_1 (s)		nT_2 (s)	NOE	T_1/T_2
		^1H 400 MHz	^1H 500 MHz	^1H 500 MHz	^1H 500 MHz	^1H 500 MHz
Backbone						
Arg[1] α	56.2	0.392 ± 0.023	0.393 ± 0.011	0.331 ± 0.035	1.410 ± 0.046	1.187 ± 0.130
Gly[2] α	44.2	0.378 ± 0.030	0.458 ± 0.017	0.421 ± 0.037	1.532 ± 0.057	1.088 ± 0.104
Asp[3] α	49.1	–	–	–	–	–
D-Pro[4] α	59.4	0.391 ± 0.023	0.424 ± 0.013	0.387 ± 0.050	1.462 ± 0.047	1.096 ± 0.145
Pro[5] α	62.5	0.433 ± 0.026	0.466 ± 0.014	0.391 ± 0.051	1.420 ± 0.044	1.192 ± 0.160
Gly[6] α	42.4	0.434 ± 0.034	0.514 ± 0.020	0.420 ± 0.035	1.477 ± 0.053	1.224 ± 0.113
Side chains						
Arg[1] β	27.8	0.429 ± 0.031	0.527 ± 0.019	0.469 ± 0.040	1.459 ± 0.048	1.124 ± 0.104
Asp[3] β	36.7	0.427 ± 0.037	0.501 ± 0.022	0.295 ± 0.025	1.538 ± 0.062	1.698 ± 0.162
D-Pro[4] β	29.4	0.667 ± 0.042	0.756 ± 0.022	0.699 ± 0.080	1.502 ± 0.045	1.082 ± 0.128
Pro[5] β	30.6	0.578 ± 0.035	0.708 ± 0.021	0.642 ± 0.066	1.410 ± 0.043	1.103 ± 0.118
Arg[1] γ	26.3	0.590 ± 0.032	0.698 ± 0.019	0.629 ± 0.059	1.575 ± 0.041	1.110 ± 0.108
D-Pro[4] γ	26.3	0.861 ± 0.045	0.976 ± 0.027	0.915 ± 0.140	1.575 ± 0.041	1.067 ± 0.166
Pro[5] γ	25.0	0.699 ± 0.046	0.716 ± 0.030	0.702 ± 0.100	1.540 ± 0.046	1.020 ± 0.151
Arg[1] δ	42.0	0.676 ± 0.038	0.738 ± 0.020	0.631 ± 0.057	1.565 ± 0.044	1.170 ± 0.110

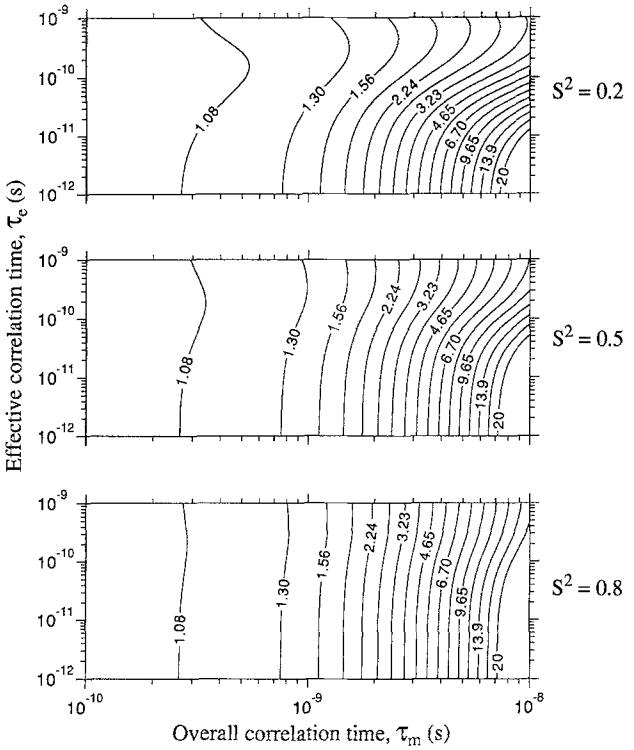

Fig. 2. T_1/T_2 ratio contour plots for a range of the effective correlation time, τ_e, and the overall correlation time, τ_m, calculated for different order parameters, S^2, at a proton resonance frequency of 500 MHz, using Eqs. 1, 2 and 7. These contour plots are useful for estimating the overall correlation time τ_m. The contour levels follow a geometric progression with a ratio between two consecutive levels of 1.20. For large ratios, as typically found for proteins, the contour levels become more closely spaced and a reasonable accuracy is achievable. For small ratios, as typically found for small peptides such as those in this study, an accurate determination of the overall correlation time is not possible, since a small displacement of the ratio may lead to a large change in the correlation time. For large order parameters and for short effective correlation times, the ratio becomes fairly independent of the internal motion. For smaller overall correlation times and medium order parameters, this is not true, and a relative dependence of the ratio on the internal correlation time τ_e can be observed.

The range for the overall correlation times τ_m was estimated by calculating the mean T_1/T_2 ratio at 500 MHz proton resonance frequency. This procedure is common for proteins and medium-sized peptides (Kay et al., 1989; Clore et al., 1990a; Palmer et al., 1991) in which the mean T_1/T_2 ratio of the backbone nuclei may yield a fairly accurate determination of τ_m. Figure 2 shows contour plots of T_1/T_2 ratios calculated from Eqs. 1 and 2 with the spectral density function of Eq. 7, including the model-free parameters. For large S^2 and τ_m on the nanosecond time scale, as typically found in proteins, it can clearly be seen that the T_1/T_2 ratio contour levels become more closely spaced and a reasonable accuracy is achievable. Furthermore, this ratio becomes very insensitive to the internal correlation time τ_e. Unfortunately, for small peptides with medium-sized S^2 and τ_m on the subnanosecond time scale, an accurate determination of the overall correlation time is not possible because a small displacement of the T_1/T_2 ratio leads to a large change in the estimate of the overall correlation time τ_m. Nevertheless, a crude estimate is sufficient as a starting point and provides a range from which a grid search with a fine grid step can easily optimize.

Error estimation of the dynamical parameters

The uncertainties in the model-free parameters were evaluated by Monte Carlo simulations. By assuming that the measured experimental data and their respective experimental errors were the mean and standard deviation of Gaussian distributions, 400 sets of experimental relaxation times and NOE enhancements were generated by randomly sampling within these distributions. For each sample, optimized dynamical parameters were calculated using the procedure described above. The reported values with their uncertainties corresponded to the average and standard deviations statistically analyzed from the 400 resulting sets of optimized values.

Results and Discussion

Relaxation data

The relaxation times and NOE enhancements for the three compounds are listed in Tables 1–3. The uncertainties estimated from the covariance matrix derived from the nonlinear fitting functions for the relaxation times were in the ranges of 4–8% for T_1 measured at 400 MHz, 2–4% for T_1 measured at 500 MHz and 6–11% for T_2 measured at 500 MHz. The uncertainties in the NOE enhancements at 500 MHz, evaluated with Eq. 8, were in the range of 2–3%. The greater uncertainties for T_1 at 400 MHz compared to those at 500 MHz are largely due to the probes that were used; at 400 MHz, an inverse probe was used whereas at 500 MHz, a broadband probe was used. The larger uncertainties obtained in the T_2 relaxation times can be attributed to a greater percentage contribution of the baseline noise to the measured peak intensity for long relaxation delays, and also to the possibility that the experimental CPMG relaxation curve is not well described by a monoexponential decay.

The very short T_2 relaxation time of the aspartate C^β of **I** was not measured by the CPMG experiment. Instead, T_2 was extracted from the observed line width by removing the exponential apodization contribution and B_0 field inhomogeneity contributions. The latter was evaluated from the other resonance peaks for which T_2 was known. The average B_0 field inhomogeneity contribution was subtracted from the line width and its standard deviation was used to calculate the experimental error in the T_2 relaxation time.

A comparison of the T_1 relaxation data for the three compounds indicates that the average T_1 relaxation times

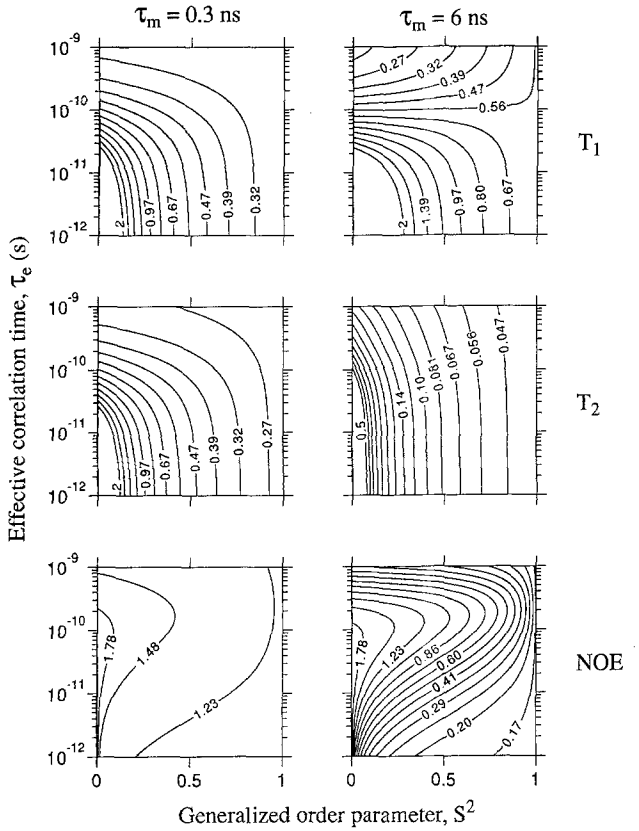

Fig. 3. Contour plots of T_1 and T_2 relaxation times, and NOE enhancement calculated at 500 MHz proton resonance frequency for overall correlation times of 0.3 and 6 ns. These two correlation times mimic the size of a small peptide and a protein, respectively. The relaxation parameters were calculated using Eqs. 1–3 with the spectral density function expressed by Eq. 7. The contour levels follow a geometric progression, with a ratio between two consecutive levels of 1.20.

for the backbone ^{13}C nuclei follows the order $\overline{T_1}(\mathbf{I}) > \overline{T_1}(\mathbf{III}) > \overline{T_1}(\mathbf{II})$. This can be qualitatively interpreted using the following equation (Fushman et al., 1994):

$$\frac{1}{T_1} = \frac{S^2}{T_1^{iso}(\tau_m)} + (1-S^2)\frac{1}{T_1^{iso}(\tau)} \qquad (10)$$

where $T_1^{iso}(\tau_m)$ and $T_1^{iso}(\tau)$, with $1/\tau = 1/\tau_m + 1/\tau_e$, correspond to the dipolar relaxation times calculated for the case of purely isotropic rotational motion with correlation times τ_m and τ, respectively. A similar description can be made for T_2 relaxation times if dipolar relaxation alone is involved. However, the average backbone T_2 values are in the order $\overline{T_2}(\mathbf{III}) > \overline{T_2}(\mathbf{II}) > \overline{T_2}(\mathbf{I})$. Decay processes other than dipolar relaxation are probably responsible for this discrepancy. A criterion for establishing if these additional processes contribute to T_2 is necessary to determine its utility for the model-free analysis. One that has proved useful for proteins and medium-sized peptides (Clore et al., 1990a; Palmer et al., 1991) is based on a statistical analysis of backbone T_1/T_2 ratios. Ratios larger by one standard deviation or more than the mean ratio are assumed to indicate additional mechanisms of line broadening, while T_1/T_2 ratios that are smaller by at least one standard deviation indicate that high-frequency internal motions contribute more significantly than average to the relaxation rates. For small peptides, like those considered here, the same criterion can be applied, but a statistical analysis restricted to backbone atoms may not be very reliable due to the small number of backbone ^{13}C nuclei studied. The T_1/T_2 ratios for backbone and side-chain carbons are listed in Tables 1, 2 and 3 for compounds **I**, **II** and **III**, respectively. The mean ratios $\overline{T_1/T_2}$ for the three compounds, if the side-chain ^{13}C nuclei are included, are: $\overline{T_1/T_2}(\mathbf{I}) = 1.26 \pm 0.08$, $\overline{T_1/T_2}(\mathbf{II}) = 1.10 \pm 0.08$, and $\overline{T_1/T_2}(\mathbf{III}) = 1.17 \pm 0.16$. For **I**, the T_1/T_2 ratios of aspartate C^α and aspartate C^β were not used for calculating $\overline{T_1/T_2}(\mathbf{I})$, because of their unusually large values, presumed a priori to originate from exchange broadening. In addition to these two nuclei of **I**, arginine C^β exhibited a ratio barely above one standard deviation from the mean value, and (L-)proline C^γ had a ratio slightly under one standard deviation from the mean value. For **II** and **III**, only the C^β of aspartate showed a T_1/T_2 ratio above at least one standard deviation from the respective mean values.

The NOE enhancement for a peptide with a subnanosecond overall correlation time of 0.3 ns is not very sensitive to internal motions when compared to a protein with an overall correlation time of 6 ns. This is illustrated in Fig. 3, which shows the calculated dependence of T_1, T_2 and NOE on τ_e and S^2 for those two values of τ_m at a proton resonance frequency of 500 MHz. Equations 1–3 were used for the calculations of Fig. 3. The only NOE enhancement which is surprisingly low when compared to the other ones corresponds to the aspartate C^β of **I** at a value of 1.249, although it is still possible to describe this NOE value within the range of dynamical parameters considered here.

Initial estimates of τ_m

As was mentioned earlier, a starting estimate for τ_m may be obtained from Fig. 2 by mapping the contour level corresponding to the mean T_1/T_2 ratio onto the τ_m axis. An order parameter S^2 of about 0.5 was used and it was assumed that $\tau_e \ll \tau_m$. The τ_m estimates for all three compounds were: (**I**) 0.7 ± 0.2 ns; (**II**) 0.3 ± 0.2 ns; and (**III**) 0.5 ± 0.4 ns. The significant discrepancies among these estimates are noteworthy, given that the three compounds are isomers; this again suggests that additional decay processes, not considered in the model-free approximation, might be present. The minimization of E^2 was thus performed over the following range: $0.1 \text{ ns} \le \tau_m \le 1$ ns.

Model-free parameters for the peptides

The optimized model-free parameters originating from

the minimization of E^2 with and without T_2 relaxation times are listed in Tables 4, 5 and 6 for compounds **I**, **II** and **III**, respectively. The minimization including T_2 relaxation times, with the exception of those exhibiting a T_1/T_2 ratio larger than at least one standard deviation from the mean T_1/T_2 ratio, yielded almost identical results as those found from the minimization excluding T_2 relaxation times, well within the uncertainties estimated by the Monte Carlo simulations. For **I**, T_2 values of aspartate C^α and C^β and arginine C^β were excluded from the search. For **II** and **III**, only aspartate C^β was excluded. Experience with including those T_2 values that are shortened by additional decay processes according to the criterion described showed that they may affect the optimization of the overall correlation time τ_m, causing it to be overestimated.

Figure 4 illustrates the experimental relaxation times and NOE enhancements for all three compounds together with the fitted values, calculated with the optimized dynamical parameters obtained by the minimization of E^2 excluding T_2 values. Most of the relaxation data are well fitted by the model-free parameters, with the clear exception of a large proportion of the T_2 values observed for **I** and the T_2 of aspartate C^β in **II** and **III**. For the latter, a discrepancy was expected since they exhibited outlying T_1/T_2 ratios. The observation that the NOE enhancements appear to have the best fit is not surprising because, as was shown in Fig. 3, the NOE enhancements are not very sensitive to the dynamical parameters for molecules experiencing overall tumbling on the subnanosecond time scale. Analysis of the minimization of E^2 yielded the following minimum values of e^2, which is E^2 divided by the number of experimental data points used in the grid search (on average, the fitted relaxation time or NOE enhancement is $\sigma\sqrt{e^2}$ away from the observed value, where σ is the experimental error; the first value is excluding T_2 values and the second is including T_2 values): (**I**) $e^2 = 0.45$ or 0.89; (**II**) $e^2 = 0.35$ or 0.38; and (**III**) $e^2 = 0.37$ or 0.41. Thus, for **I**, e^2 doubles in value when T_2 relaxation times are included in the minimization of E^2, whereas for **II** and **III**, e^2 remains essentially constant. Since inclusion or exclusion of all T_2 data produced nearly identical results for the predicted T_1 and NOE values, the increase in e^2 observed for **I** must arise from the discrepancy between the experimental and fitted T_2 values seen in Fig. 4. Thus, the T_1/T_2 criterion used to exclude from the grid search those T_2 relaxation times that experience line broadening was useful but, not unexpectedly, insufficient in a case where a majority of nuclei experience some form of line broadening. On the other hand, the minimization of E^2 with inclusion of T_2 values did not affect the optimization of τ_m, since identical values to within 0.01 ns were found whether or not T_2 data was included.

The backbone and side-chain order parameters S^2 for all three compounds, obtained with the minimization of E^2 excluding T_2 values, are displayed in column charts in Fig. 5. As indicated earlier, data for aspartate C^α of **III** could not be obtained. The mean values, $\overline{S^2}$, for the backbone and side-chain nuclei are also shown. Their standard deviations, σ_{S^2}, which are useful for evaluating their relative dispersion, are: (**I**) $\sigma_{S^2} = 0.07$ (backbone), $\sigma_{S^2} = 0.07$ (side chain); (**II**) $\sigma_{S^2} = 0.08$ (backbone), $\sigma_{S^2} = 0.06$ (side chain); and (**III**) $\sigma_{S^2} = 0.07$ (backbone), $\sigma_{S^2} = 0.09$ (side chain). For each peptide the S^2 values of the glycine C^α

TABLE 4
MODEL-FREE DYNAMICAL PARAMETERS FOR cyclo(Arg-Gly-Asp-Gly-D-Pro-Pro) (**I**)

Residue	S^2		τ_e (ps)		R_{ex} (s^{-1})		E_i^2	
	without T_2	with T_2	without T_2	with T_2	without T_2	with T_2	without T_2	with T_2
Backbone								
Arg^1 α	0.53±0.07	0.53±0.07	79±21	81±20	0.45±0.42	0.43±0.40	0.89	2.48
Gly^2 α	0.37±0.05	0.38±0.05	65±14	70±14	0.50±0.22	0.42±0.19	0.18	6.51
Asp^3 α	0.51±0.07	0.50±0.07	70±21	71±20	3.27±0.46	3.27±0.46	0.17	0.17[a]
Gly^4 α	0.34±0.05	0.34±0.05	58±12	60±12	0.29±0.21	0.25±0.18	0.07	2.22
D-Pro^5 α	0.43±0.06	0.43±0.06	76±16	77±15	0.41±0.38	0.40±0.37	2.94	4.15
Pro^6 α	0.37±0.05	0.37±0.05	71±13	73±13	0.61±0.38	0.58±0.37	2.24	6.20
Side chains								
Arg^1 β	0.29±0.05	0.29±0.04	86±11	87±11	0.76±0.25	0.76±0.25	1.30	1.30[a]
Asp^3 β	0.45±0.06	0.45±0.06	12±6	12±6	23.7 ±3.4	23.7 ±3.4	0.67	0.63[a]
D-Pro^5 β	0.27±0.03	0.27±0.03	48±8	49±8	0.25±0.19	0.23±0.17	0.91	2.92
Pro^6 β	0.23±0.03	0.24±0.03	32±5	32±5	0.29±0.16	0.27±0.15	0.57	4.67
Arg^1 γ	0.22±0.03	0.23±0.03	61±7	63±7	0.28±0.17	0.25±0.16	0.11	2.88
D-Pro^5 γ	0.27±0.03	0.27±0.03	32±7	33±7	0.27±0.19	0.25±0.17	5.08	7.82
Pro^6 γ	0.25±0.03	0.25±0.03	16±5	16±5	–	–	1.64	1.81
Arg^1 δ	0.22±0.03	0.22±0.03	59±7	60±7	0.18±0.18	0.17±0.16	2.14	3.54

$\tau_m = 0.29 \pm 0.02$ ns (without T_2); $\tau_m = 0.29 \pm 0.02$ ns (with T_2).
[a] T_2 relaxation times were excluded from the search.

TABLE 5
MODEL-FREE DYNAMICAL PARAMETERS FOR cyclo(Arg-Gly-Asp-D-Pro-Gly-Pro) (**II**)

Residue	S^2		τ_e (ps)		R_{ex} (s^{-1})		E_i^2	
	without T_2	with T_2	without T_2	with T_2	without T_2	with T_2	without T_2	with T_2
Backbone								
Arg[1] α	0.49±0.09	0.49±0.10	180±38	182±37	–	–	1.31	1.56
Gly[2] α	0.52±0.06	0.52±0.07	42±17	43±19	–	–	0.17	0.94
Asp[3] α	0.70±0.09	0.70±0.11	71±38	74±42	0.32±0.19	0.30±0.18	1.23	4.29
D-Pro[4] α	0.63±0.07	0.62±0.09	46±25	48±27	–	–	0.30	0.47
Gly[5] α	0.49±0.07	0.49±0.08	88±22	89±23	–	–	4.29	4.38
Pro[6] α	0.64±0.07	0.63±0.08	43±24	45±26	–	–	0.21	0.40
Side chains								
Arg[1] β	0.36±0.05	0.36±0.06	82±12	83±13	–	–	0.37	1.10
Asp[3] β	0.23±0.04	0.23±0.04	83±9	84±9	0.57±0.12	0.57±0.12	0.44	0.49[a]
D-Pro[4] β	0.35±0.03	0.35±0.04	14±6	15±8	–	–	0.05	0.20
Pro[6] β	0.31±0.03	0.31±0.04	23±6	24±7	–	–	0.09	0.20
Arg[1] γ	0.30±0.03	0.29±0.04	43±7	44±7	–	–	0.09	0.24
D-Pro[4] γ	0.24±0.03	0.23±0.03	26±5	27±6	–	–	0.41	0.56
Pro[6] γ	0.20±0.02	0.20±0.03	27±4	28±4	–	–	0.07	0.25
Arg[1] δ	0.19±0.03	0.19±0.03	60±5	60±5	–	–	5.60	5.84

$\tau_m = 0.26 \pm 0.02$ ns (without T_2); $\tau_m = 0.26 \pm 0.03$ ns (with T_2).
[a] T_2 relaxation times were excluded from the search.

atoms are smaller than the backbone $\overline{S^2}$, consistent with the absence of a side chain to limit internal motion. It is very clear from Fig. 5 and the mean backbone values for the three compounds, 0.43 (**I**), 0.58 (**II**) and 0.53 (**III**), that the backbone of compound **I** exhibits the highest degree of internal mobility on the subnanosecond time scale, and that compound **II** probably has the most rigid backbone on this time scale. This result is fully consistent with the results of the previously reported constrained static conformational searches as illustrated in Fig. 1.

The side-chain $\overline{S^2}$ values, as expected, are generally lower than those for the backbone. They are in general not very clearly distinguished, except that aspartate C^β of **I** is an obvious outlier in this peptide; we shall return to this point later.

The mean values of τ_e for the backbone and side-chain nuclei with their respective standard deviation σ_{τ_e}, obtained with the minimization of E^2 excluding T_2 values, are the following: (**I**) $\overline{\tau_e} = 70 \pm 7$ ps (backbone), $\overline{\tau_e} = 43 \pm 23$ ps (side chain); (**II**) $\overline{\tau_e} = 78 \pm 48$ ps (backbone), $\overline{\tau_e} = 45 \pm 25$

TABLE 6
MODEL-FREE DYNAMICAL PARAMETERS FOR cyclo(Arg-Gly-Asp-D-Pro-Pro-Gly) (**III**)

Residue	S^2		τ_e (ps)		R_{ex} (s^{-1})		E_i^2	
	without T_2	with T_2	without T_2	with T_2	without T_2	with T_2	without T_2	with T_2
Backbone								
Arg[1] α	0.64±0.06	0.64±0.06	48±28	49±28	0.37±0.30	0.35±0.28	2.18	3.49
Gly[2] α	0.46±0.06	0.46±0.06	80±22	81±21	–	–	1.69	1.70
Asp[3] α	–	–	–	–	–	–	–	–
D-Pro[4] α	0.54±0.06	0.54±0.06	67±25	68±25	–	–	0.04	0.09
Pro[5] α	0.54±0.05	0.54±0.06	33±19	34±19	–	–	0.15	0.94
Gly[6] α	0.45±0.06	0.46±0.06	45±19	47±20	0.31±0.23	0.26±0.20	0.22	2.83
Side chains								
Arg[1] β	0.47±0.05	0.47±0.05	35±16	36±17	–	–	2.05	2.13
Asp[3] β	0.40±0.07	0.40±0.07	68±22	68±22	1.27±0.30	1.27±0.30	0.69	0.69[a]
D-Pro[4] β	0.29±0.03	0.29±0.03	25±7	25±8	–	–	0.33	0.35
Pro[5] β	0.37±0.02	0.37±0.02	13±5	13±5	–	–	2.40	2.41
Arg[1] γ	0.27±0.03	0.27±0.03	42±8	42±8	–	–	2.50	2.62
D-Pro[4] γ	0.19±0.02	0.19±0.02	25±5	25±5	–	–	0.77	0.78
Pro[5] γ	0.27±0.04	0.27±0.04	33±9	33±9	–	–	1.55	1.55
Arg[1] δ	0.26±0.04	0.26±0.04	36±8	37±8	0.17±0.16	0.16±0.15	0.04	1.35

$\tau_m = 0.26 \pm 0.01$ ns (without T_2); $\tau_m = 0.26 \pm 0.01$ ns (with T_2).
[a] T_2 relaxation times were excluded from the search.

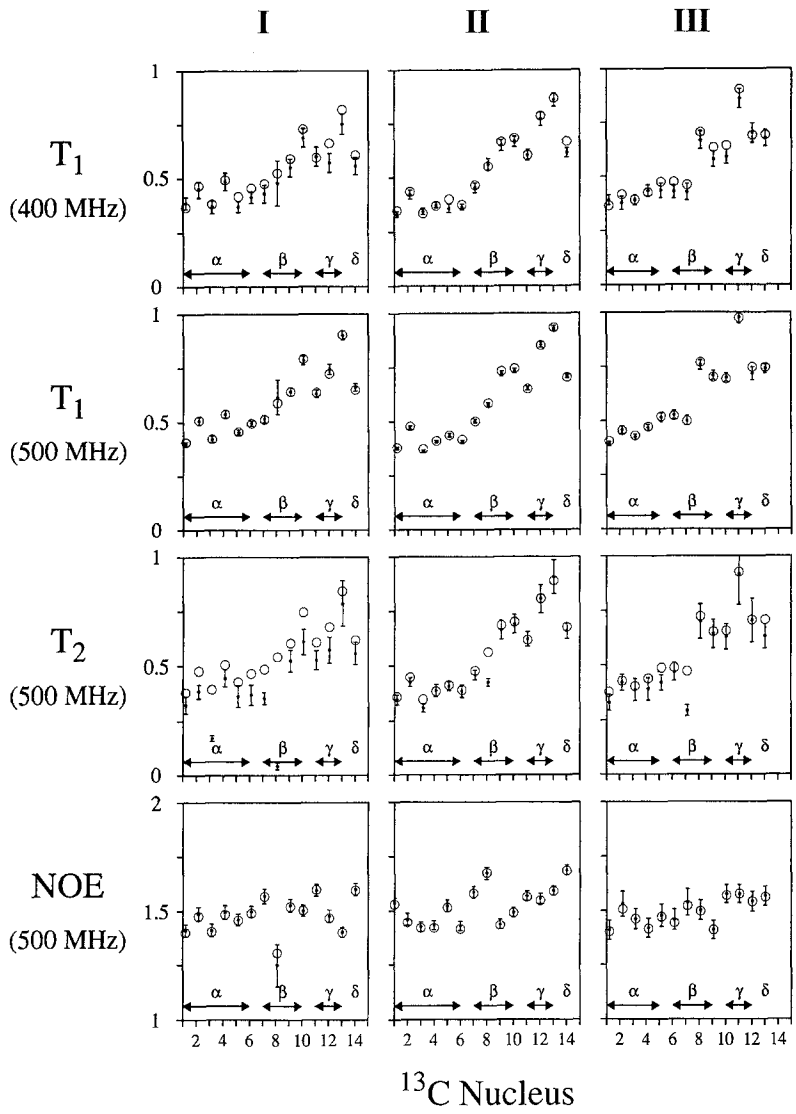

Fig. 4. Experimental relaxation times and NOE enhancements versus their fitted values, which were calculated with the optimized model-free parameters (without T_2) of Tables 4–6. The circles represent the calculated values, whereas the dots and their respective error bars represent the experimental values. The ^{13}C nucleus ordering corresponds to the same nucleus ordering as listed in Tables 1–6. The α-nuclei correspond to the backbone ^{13}C nuclei, whereas all the other ones correspond to the side-chain ^{13}C nuclei.

ps (side chain); and (**III**) $\overline{\tau_e} = 54 \pm 17$ ps (backbone), $\overline{\tau_e} = 35 \pm 15$ ps (side chain). For all three compounds, the average internal correlation time experienced by the backbone nuclei is about 1.6 times longer than those, on average, experienced by the side-chain ^{13}C nuclei.

Validity of the model-free analysis

The model-free analysis had not previously been reported for molecules as small as these cyclic hexapeptides, for which the overall molecular correlation time is very close to the time scale of the internal motions. Therefore we investigated its applicability in this regime.

Use of T_1 and T_2 relaxation times and NOE enhancements for extracting the model-free parameters, measured at the same field strength or at different field strengths, requires that these relaxation parameters experience a different and unique dependence on the dynamical parameters. Figure 3 illustrates the dependence of the relaxation parameters on the internal dynamical parameters S^2 and τ_e for two overall correlation times, 0.3 and 6 ns, which mimic a small peptide and a protein, respectively. The contour level patterns for T_1 and T_2 at $\tau_m = 0.3$ ns are quite similar, whereas those at $\tau_m = 6$ ns are significantly different over most of the range. However, within much of the observable range discussed previously, $0.1\tau_m < \tau_e < 10\tau_m$, T_1 and T_2 relaxation times for $\tau_m = 0.3$ ns are sensitive to changes in the internal correlation time τ_e. For $\tau_m = 6$ ns, on the other hand, it is known (Kay et al., 1989; Clore et al., 1990a; Palmer et al., 1991) that for large S^2, which are typical for proteins, T_1 and T_2 relaxation times are fairly insensitive to the internal correlation time τ_e. This is clearly illustrated in Fig. 3. Finally, the

NOE enhancement is relatively insensitive to the dynamical parameters at $\tau_m = 0.3$ ns, while the NOE enhancement at $\tau_m = 6$ ns exhibits a closely spaced set of contour levels. These differences have an impact on the accuracy obtained for the model-free parameters that is not simple to predict. Work is in progress to address this issue analytically for molecules experiencing overall rotational tumbling on the subnanosecond time scale.

For the present case, the uncertainties in the dynamical parameters were calculated from 400 sets of optimized model-free parameters obtained by Monte Carlo simulations as described in the section Experimental Methods, and they are reported with the parameters in Tables 4–6 and Fig. 5. The nearly identical results and uncertainties obtained with or without T_2 relaxation times in the minimization of E^2 is a clear indication that the exclusion of T_2 values does not significantly under-determine the system. Otherwise this could have translated into much larger uncertainties in the derived dynamical parameters, and it could lead to over-interpretation. It is very likely that the inclusion of T_1 relaxation times measured at a different field strength did help in creating a different and unique dependence on the dynamical parameters, thereby preventing potential instabilities in the Monte Carlo simulations.

The uncertainties in S^2 for the backbone and side-chain ^{13}C nuclei of all three compounds were found to lie in the range of 11–14%, so that the conclusion reached above about the relative internal mobilities of the three peptides is likely to be valid. The uncertainties in the effective correlation times τ_e were on average larger for the backbone ^{13}C nuclei than for the side-chain ^{13}C nuclei. They ranged between 23–41% for the backbone τ_e and between 15–29% for the side-chain τ_e. The greater uncertainty for the backbone is expected, since for larger values of S^2, the T_1 and T_2 relaxation times become less sensitive to τ_e.

Chemical exchange

Decay processes other than dipolar relaxation, contributing to the transverse relaxation of the ^{13}C nuclei, were summed up in an R_{ex} term (Eq. 4), which was extracted by subtracting the predicted value of T_2 (dipolar), calculated with the optimized model-free parameters, from the observed transverse relaxation rate. The uncertainties in R_{ex} were estimated by the Monte Carlo simulations. Those R_{ex} contributions to transverse relaxation that were larger than the experimental error in the observed transverse rates $1/T_2$ are listed with their uncertainties in Tables 4–6.

Examination of the R_{ex} contributions reveals that there is a chemical exchange process involving the aspartate side chains of all three peptides, but most strongly manifested in compound **I**. A second, less specific, exchange process, presumably related to overall conformational changes at microsecond rates, appears to be unique for **I**.

The chemical exchange process taking place at aspartate presumably arises from an interaction of its carboxylate group, most likely an equilibrium that involves making and breaking of an intramolecular hydrogen bond. An exchange equilibrium with the solvent, though less likely, is not ruled out. Involvement of a side-chain–backbone hydrogen bond is suggested for **I**, at least, by the much higher than average order parameter for its

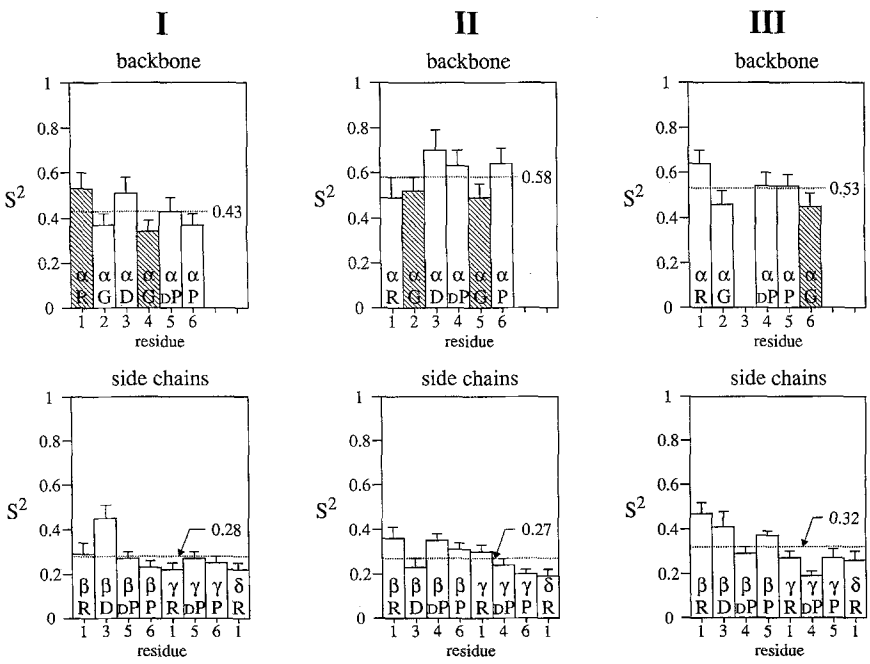

Fig. 5. Column chart of the optimized order parameters S^2 (without T_2) along the backbone and on the side chains for compounds **I**, **II** and **III**. The shaded areas in the top views correspond to the residues that are involved in intramolecular hydrogen bonds across the β-turns.

aspartate C^{β} (Fig. 5). A very rough estimate of the rate range of this process is possible on the basis of the two-site, equal population exchange model (Gutowsky et al., 1953; Bloom et al., 1965) with the further assumption, solely for the sake of estimation, that the chemical shift difference between the C^{β} sites in all three cases is of the order of 4 ppm, which is the difference between ionized and unionized side chains (Silverstein et al., 1981). Then the estimated exchange lifetimes, τ_{ex}, calculated with $\tau_{ex} = 2R_{ex}/\omega_{ex}^2$, where $\tau_{ex} = 1/k_{ex}$ has been used in Eq. 4, are in the microsecond region, ranging from 5×10^{-6} s for **I** to 10^{-7} s for **II**.

The general chemical exchange process observed in **I** produces roughly the same order of R_{ex} across the backbone and the side chains. If we focus on the R_{ex} of the backbone nuclei and calculate the average R_{ex}, excluding the outlying aspartate C^{α}, we obtain $\overline{R_{ex}} = 0.45\ s^{-1}$. If the two-site exchange process with equal population is again assumed, a characteristic exchange lifetime, τ_{ex}, can be estimated, given a guess for the chemical shift difference between the two exchanging sites. The average of the six standard deviations calculated for every set of three C^{α} chemical shifts (extracted from compounds **I**, **II** and **III**) was used, i.e., $\omega_{ex} = 1.3 \pm 0.6$ ppm. The resulting estimate of the exchange lifetime is $4\times10^{-7}\ s \le \tau_{ex} \le 3\times10^{-6}$ s. Using the same estimate of the chemical shift difference for the process reflected by R_{ex} contributions at Gly-Arg of **III** (Table 6), an exchange lifetime of $3\times10^{-7}\ s \le \tau_{ex} \le 2\times10^{-6}$ s was estimated, using $\overline{R_{ex}} = 0.34\ s^{-1}$.

Attempts were made to obtain additional information about these slower processes, using spin-lock experiments on **I**. The experiment was a $T_{1\rho}$ measurement in which only two rf field strengths, ω_{1a} and ω_{1b}, were sampled and only one spin-lock pulse length t_{SL} was used. This pair of experiments was repeated for each backbone ^{13}C resonance peak, and the ratio f of the two resulting resonance peak intensities was calculated. Assuming that $J(\omega_{1a}) \approx J(\omega_{1b})$, the dipolar relaxation contributions cancel, and only the $T_{1\rho}$ exchange terms (Deverell et al., 1970) contribute to the ratio. An observability condition can then be defined for the exchange lifetime τ_{ex} to cause f to depart from unity beyond its uncertainty σ_f, see Eq. 11:

$$\frac{p_1 p_2 \tau_{ex} (\omega_{ex})^2}{1+\omega_{1b}^2\tau_{ex}^2} - \frac{p_1 p_2 \tau_{ex} (\omega_{ex})^2}{1+\omega_{1a}^2\tau_{ex}^2} = \frac{\ln(f)}{t_{SL}} \ge \frac{\ln(\sigma_f)}{t_{SL}} \qquad (11)$$

Assuming equal populations and the earlier estimate of $\omega_{ex} = 1.3$ ppm, and given the experimental rf field strengths $\omega_{1a}/2\pi = 5000$ Hz and $\omega_{1b}/2\pi = 1250$ Hz, and the spin-lock period $t_{SL} = 0.15$ s with an uncertainty of 3% in measured intensity ($\sigma = 0.03$), the intensity ratio remains unity within its experimental error, unless $\tau_{ex} > 10\times10^{-6}$ s. We conclude that for the backbone of **I** there are no significant processes slower than $10^5\ s^{-1}$. No further $T_{1\rho}$ experiments were pursued.

Conclusions

In summary, the internal motions of three isomeric cyclic hexapeptides were examined experimentally, by measurement of ^{13}C relaxation parameters, T_1 at 400 and 500 MHz, and T_2 and nuclear Overhauser enhancements at 500 MHz. These were interpreted according to the model-free formalism of Lipari and Szabo, which is usually applied to data from macromolecules and larger sized peptides to yield information about internal motions on the 10–100 ps time scale. The applicability of the model-free analysis with acceptable uncertainties to these small, six-residue peptides, with overall rotational correlation times slightly below 0.3 ns, was demonstrated for this specific instance. Chemical exchange contributions to T_2 from slower motions were also identified in the process.

The peptides examined, cyclo(Arg-Gly-Asp-Gly-D-Pro-Pro) (**I**), cyclo(Arg-Gly-Asp-D-Pro-Gly-Pro) (**II**) and cyclo(Arg-Gly-Asp-D-Pro-Pro-Gly) (**III**), were designed using proline residues to stabilize particular versions of the common two-β-turn cyclic hexapeptide backbone format. Studies using a distance geometry conformational search restricted by experimental NOE and coupling constant constraints confirmed that the designed two-turn conformations were maintained in solution. However, although the data and search very narrowly defined the conformation of **II**, there was a large uncertainty indicated in the conformation about the Gly-Asp turn of **I**, and two probable conformations were indicated for the Arg-Gly turn of **III**. The result of the present dynamic study of these molecules is that, according to the order parameters obtained for its backbone α-carbon atoms, **II** indeed has the most rigid backbone conformation on the 10–100 ps time scale, and **I** the most flexible. This parallelism is not an obvious expectation, and a similar parallelism between experimental dynamics and static conformational uncertainty need not be expected for other cases. It will thus be of considerable interest to perform similar studies with other sets of closely related cyclic peptides.

In some cyclic peptide systems, proton $T_{1\rho}$ measurements have demonstrated backbone motion in the 10–50 μs range (Kopple et al., 1988; Blackledge et al., 1993). This is frequently associated with rotation of an amide plane relative to the overall ring plane. The present study appears to indicate that at least in **I**, which now safely may be termed the most flexible of the three peptides, there is backbone motion that is likely to be in the 1 μs region, where it is not readily reflected in relaxation parameters.

No attempt was made to extract motional information such as order parameters (Chen et al., 1994) from the ensemble of likely conformations originating from the NOE distance constraints (Fig. 1) and to compare them with the results of the dynamic study. The NOE distance constraints may have been affected by additional internal

motions lying outside the time scale that was probed in our study. Furthermore, the range of likely conformations generated from NOE distance constraints may be influenced by possible incompleteness of the NOE data set.

From the standpoint of designing conformationally defined cyclic peptides containing β-turns, the present results, taken together with the original studies of **I**, **II** and **III**, add weight to the following generalizations. While the sequence D-Pro-L-Pro incorporated into a cyclic hexapeptide may itself adopt a well-defined type II β-turn, this turn alone does not rigidify the peptide ring to the extent of locking in a conformation for the opposite turn. The second turns of **I** and **III** of course contain glycine residues, and greater rigidity may be expected when both residues are substituted. The turns of **II**, both of which contain proline and a substituted residue, are in fact conformationally stable, as is the ring containing them. Given one glycine residue in a β-turn, however, greater conformational stability appears to be achieved when a substituted residue is in the i+1 position, consistent with very early observations on the conformations of cyclo(Gly-Gly-Xxx)$_2$ systems (Kopple et al., 1972).

Acknowledgements

We are grateful to Dr. Fadia Ali, who synthesized the three compounds that were used in this study. We also thank Dr. Catherine E. Peishoff for the preparation of Fig. 1.

References

Abragam, A. (1961) *Principles of Nuclear Magnetism*, Clarendon Press, Oxford, pp. 264–353.

Ali, F.E. and Samanen, J.M. (1992) In *Innovations and Perspectives in Solid Phase Synthesis: Peptides, Polypeptides and Oligonucleotides* (Ed., Epton, R.), Intercept Ltd., Hanover, U.K., pp. 333–335.

Barbato, G., Ikura, M., Kay, L.E., Pastor, R.W. and Bax, A. (1992) *Biochemistry*, **31**, 5269–5278.

Bean, J.W., Kopple, K.D. and Peishoff, C.E. (1992) *J. Am. Chem. Soc.*, **114**, 5328–5334.

Bevington, P.R. (1969) *Data Reduction and Error Analysis for the Physical Sciences*, McGraw-Hill Inc., New York, NY.

Blackledge, M.J., Brüschweiler, R., Griesinger, C., Schmidt, J.M., Xu, P. and Ernst, R.R. (1993) *Biochemistry*, **32**, 10960–10974.

Bloom, M., Reeves, L.W. and Wells, E.J. (1965) *J. Chem. Phys.*, **42**, 1615–1624.

Bonvin, A.M.J.J., Boelens, R. and Kaptein, R. (1993) In *Computer Simulation of Biomolecular Systems: Theoretical and Experimental Applications*, Vol. 2 (Eds, Van Gunsteren, W.F., Weiner, P.K. and Wilkinson, A.J.), ESCOM, Leiden, pp. 407–440.

Bremi, T., Ernst, M. and Ernst, R.R. (1994) *J. Phys. Chem.*, **98**, 9322–9334.

Carr, H.Y. and Purcell, E.M. (1954) *Phys. Rev.*, **94**, 630–638.

Chen, Y., Suri, A.K., Kominos, D., Sanyal, G., Naylor, A.M., Pitzenberger, S.M., Garsky, V.M., Levy, R.M. and Baum, J. (1994) *J. Biomol. NMR*, **4**, 307–324.

Clore, G.M., Driscoll, P.C., Wingfield, P.T. and Gronenborn, A.M. (1990a) *Biochemistry*, **29**, 7387–7401.

Clore, G.M., Szabo, A., Bax, A., Kay, L.E., Driscoll, P.C. and Gronenborn, A.M. (1990b) *J. Am. Chem. Soc.*, **112**, 4989–4991.

Dellwo, M.J. and Wand, A.J. (1989) *J. Am. Chem. Soc.*, **111**, 4571–4578.

Deverell, C., Morgan, R.E. and Strange, J.H. (1970) *Mol. Phys.*, **18**, 553–559.

Fushman, D., Weisemann, R., Thüring, H. and Rüterjans, H. (1994) *J. Biomol. NMR*, **4**, 61–78.

Gutowsky, H.S., McCall, D.M. and Slichter, C.P. (1953) *J. Chem. Phys.*, **21**, 279–292.

Jarvis, J.A. and Craik, D.J. (1995) *J. Magn. Reson. Ser. B*, **107**, 95–106.

Kay, L.E., Torchia, D.A. and Bax, A. (1989) *Biochemistry*, **28**, 8972–8979.

Kay, L.E., Nicholson, L.K., Delaglio, F., Bax, A. and Torchia, D.A. (1992) *J. Magn. Reson.*, **97**, 359–375.

King, R. and Jardetzky, O. (1978) *Chem. Phys. Lett.*, **55**, 15–18.

Kopple, K.D., Go, A., Logan, R.H. and Savrda, J. (1972) *J. Am. Chem. Soc.*, **94**, 973–981.

Kopple, K.D., Wang, Y.-S., Cheng, A.G. and Bhandary, K.K. (1988) *J. Am. Chem. Soc.*, **110**, 4168–4176.

Lipari, G. and Szabo, A. (1980) *Biophys. J.*, **30**, 489–506.

Lipari, G. and Szabo, A. (1982) *J. Am. Chem. Soc.*, **104**, 4545–4570.

Meiboom, S. and Gill, D. (1958) *Rev. Sci. Instrum.*, **29**, 688–691.

Neuhaus, D. and Williamson, M.P. (1989) *The Nuclear Overhauser Effect in Structural and Conformational Analysis*, VCH Publishers Inc., New York, NY, pp. 23–61.

Palmer III, A.G., Rance, M. and Wright, P.E. (1991) *J. Am. Chem. Soc.*, **113**, 4371–4380.

Palmer III, A.G., Skelton, N.J., Chazin, W.J., Wright, P.E. and Rance, M. (1992) *Mol. Phys.*, **75**, 699–711.

Palmer III, A.G., Hochstrasser, R.A., Millar, D.P., Rance, M. and Wright, P.E. (1993) *J. Am. Chem. Soc.*, **115**, 6333–6345.

Peishoff, C.E., Ali, F.E., Bean, J.W., Calvo, R., D'Ambrosio, C.A., Eggleston, D.S., Hwang, S.M., Kline, T.P., Koster, P.F., Nichols, A., Powers, D., Romoff, T., Samanen, J.M., Stadel, J., Vasko, J.A. and Kopple, K.D. (1992) *J. Med. Chem.*, **35**, 3962–3969.

Peng, J.W., Thanabal, V. and Wagner, G.J. (1991) *J. Magn. Reson.*, **95**, 421–427.

Peng, J.W. and Wagner, G. (1992a) *Biochemistry*, **31**, 8571–8586.

Peng, J.W. and Wagner, G. (1992b) *J. Magn. Reson.*, **98**, 308–332.

Press, W.H., Flannery, B.P., Teukolsky, S.A. and Vetterling, W.T. (1986) *Numerical Recipes*, Cambridge University Press, Cambridge, pp. 498–546.

Richarz, R., Nagayama, K. and Wüthrich, K. (1980) *Biochemistry*, **19**, 5189–5196.

Schneider, D.M., Dellwo, M.J. and Wand, A.J. (1992) *Biochemistry*, **31**, 3645–3652.

Shaka, A.J., Keeler, J., Frenkiel, T. and Freeman, R. (1983) *J. Magn. Reson.*, **53**, 335–338.

Silverstein, R.M., Bassler, G.C. and Morrill, T.C. (1981) *Spectrometric Identification of Organic Compounds*, 4th ed., Wiley, New York, NY, pp. 249–281.

Stone, M.J., Fairbrother, W.J., Palmer, A.G., Reizer, J., Saier, M.H. and Wright, P.E. (1992) *Biochemistry*, **31**, 4394–4406.

Vold, R.L., Waugh, J.S., Klein, M.P. and Phelps, D.E. (1968) *J. Chem. Phys.*, **48**, 3831–3832.

Williams, R.J.P. (1989) *Eur. J. Biochem.*, **183**, 479–497.

Zieger, G. and Sterk, H. (1992) *Magn. Reson. Chem.*, **30**, 387–392.